Journal of Applied Electrochemistry **31**: 85–92, 2001.

The inhibiting effect of quaternary phosphine on Ni–P alloys in 1 M H_2SO_4

S.O. NIASS[1]*, M. EBN TOUHAMI[1], N. HAJJAJI[1], A. SRHIRI[1] and H. TAKENOUTI[2]
[1]*Laboratoire d'Electrochimie et des Etudes de Corrosion, Ibn Tofail University, Faculty of Sciences, BP 133, Kenitra 14000, Morocco*
[2]*UPR 15 of CNRS, Laboratoire de Physique des Liquides et Electrochimie, P&M Curie University, CP 133, 4 place Jussieu, 75252 Paris Cedex 05, France*
*(*author for correspondence, e-mail: syoniass@hotmail.com)*

Received 17 August 1999; accepted in revised form 20 July 2000

Key words: alkyl triphenyl phosphonium, electrochemical impedance spectroscopy, electroless nickel, polarization curve

Abstract

Polarization curves, electrochemical impedance measurements and SEM analysis were used to study the dissolution and the inhibition of nickel–phosphorous alloys in 1 M H_2SO_4. The alloy specimen was obtained by electroless plating on copper substrates. The inhibiting effect of triphenyl-alkyl (C_6)-phosphonium (P_3AP) was examined. The shape of the polarization curves remained essentially unchanged by addition of the inhibitor, but the current density values decreased significantly in both the anodic and the cathodic domains. The impedance spectra at open circuit potential obtained for various immersion times showed that the dissolution of this alloy was characterized by three capacitive loops. The loops were barely distinguishable at short immersion times, but, in contrast, they appeared clearly when the specimens were left in aggressive medium for one day. Tafel extrapolation in the cathodic region gave a corrosion inhibition efficiency of 90%. In the anodic domain, the current plateau decreased approximately 100 fold as a result of inhibitor addition. The phenomenon leading to the formation of this plateau is more likely related to a film growth process than to a diffusion limitation.

1. Introduction

Nickel–metalloid alloys (P, S and/or B) are often deposited on metals such as steel, zinc and copper to improve corrosion, abrasion and erosion resistance, or merely to give an attractive aspect to metallic objects. The quality of plating may be characterized by its adherence to substrate, porosity, ductility, homogeneity and alloy composition. The concentration of metalloids depends not only on the bath composition, but also on the conditions of chemical deposition.

The corrosion-fatigue resistance of AISI 1045 in 0.5 M NaCl is increased by deposition of a 20 μm thick electroless nickel coating containing approximately 10% phosphorous [1]. Revesz et al. found Ni–P coating to be more resistant than electrodeposited nickel. This observation is not surprising as amorphous films have greater corrosion resistance than their crystalline counterpart [2].

There has been a significant effort devoted to understanding the role of the metalloid elements on the anodic behaviour of transition metal–metalloid alloys. For Ni–P alloys, Marcus and Oda showed that in an acidic medium, phosphorus is oxidized to phosphate and hinders the formation of a protective NiO film [3]. Jones et al. examined the structure of Ni–P alloys obtained electrochemically and chemically, and found that phosphorus is located in the vicinity of grain boundaries.and causes the metal to passivate [4]. According to Diegle et al., phosphorus inhibits the dissolution of nickel at primary sites, but this blocking effect is a strong function of the applied electrode potential [5]. These authors proposed a chemical passivation mechanism (formation of a protective nickel phosphate layer) where solvents played a crucial role. The corrosion of Ni–P alloys in 5% NaCl solution by analysing the polarization curves and electrochemical impedance spectroscopy (EIS) was studied by Zeller [6] who found that, at the open-circuit potential, the corrosion rate is reduced due to a marked decrease of the cathodic reaction rate. In contrast, Diegle's model of chemical passivation predicted the corrosion rate to be limited by mass transfer.

Cadet et al. compared the influence of phosphorus and boron on glassy iron electrodes prepared by the spin-quenching method [7]. These authors concluded that phosphorus is oxidized into P^{5+}, and they also emphasized that the anodic behaviour of iron depends more closely on the chemistry of alloying elements rather than on its crystallographic structure.

Recent publications explored the influence of temperature and solution composition on the autocatalytic

deposition of Ni–Cu–P and Ni–P alloys [8, 10] and on the kinetic mechanism of this process in ammonium solutions [9, 11].

In spite of these numerous studies, the corrosion mechanism of Ni–P alloys in sulfuric acid medium is not well known. The aim of the present paper is to study the corrosion of this alloy in 1 M H_2SO_4 and to characterize the influence of a corrosion inhibitor based on phosphine on the corrosion behaviour of Ni–P alloys obtained by electroless plating.

2. Experimental conditions

2.1. *Electrodes*

The copper electrodes consisted of rectangular plates 10 mm × 5 mm (0.5 cm^2) with a metallic shaft for current collection. The backside and edges of electrodes were covered with varnish. Ni–P alloy was deposited on this electrode by a chemical-plating bath [10, 11]. The solution composition used is given in Table 1. This Ni–P alloy was amorphous, adherent, bright, but porous according to SEM analysis. The plating was performed at 80 °C in a solution stirred with magnetic bar. The phosphorus content was 14.5% according to EDX analysis.

The reference electrode was saturated calomel (SCE), unless otherwise stated. A platinum gauze of large surface area was used as the counter electrode.

2.2. *Test solution*

The test solution in which the Ni–P electrode was immersed for corrosion experiments was 1 M H_2SO_4 prepared from distilled water and concentrated acid (Merck, analytical grade). The solution was open to air, was held at room temperature (20 ± 1 °C), and was agitated slowly with a magnetic bar.

2.3. *Corrosion inhibitor*

The organic compound tested as corrosion inhibitor was synthesized by the authors using a catalytic phase-transfer method [12]. The product (P_3AP) was purified by recrystallization in water and characterized by infrared, ^1H nuclear magnetic resonance (NMR) spectroscopy and microanalysis methods. The product yield was 83%.

2.4. *Electrochemical measurements*

The polarization curves were obtained in a three-electrode cell connected to a potentiostat (EG&G, model 6310). Experiments were monitored by a personal computer with software supplied by EG&G. Electrochemical impedance spectroscopy (EIS) was measured with the same equipment by software versions M398 or M352. The amplitude of the a.c. signal was 5 mV (r.m.s.) and the frequency range was 100 kHz to 10 mHz using five points per decade.

Table 1. Solution composition for Ni–P plating (mol L^{-1})

$NiSO_4$	Hypophosphite	Citrate	Sodium gluconate	pH
0.1	0.28	0.2	0.046	5

The Ni–P alloy electrode was, prior to experiments, washed by acetone followed by ethanol and air-dried. The electrode was set vertically in the electrochemical cell. It was maintained in the test solution for one hour before any measurements, unless otherwise stated. The polarization curve was measured from the open circuit corrosion potential to more cathodic or to more anodic potentials at a sweep rate of 0.5 mV s^{-1}. The two branches were therefore obtained by two independent experiments.

3. Results and discussion

The results obtained in 1 M H_2SO_4 solution without inhibitor and with P_3AP inhibitor are presented below.

3.1. *Solution without inhibitor*

Impedance and polarization curves are presented in this section at the open circuit potential and in both anodic and cathodic potential domains.

3.1.1. *EIS results at the open-circuit potential*

The impedance response,obtained after one-hour of immersion in 1 M H_2SO_4 is presented in Figure 1(a). The impedance diagram shows a capacitive behavior throughout the measured frequency range; however, it is difficult to determine the number of time constants involved in this loop. A careful examination of this diagram reveals a slight change of curvature near 10 Hz. This point is more evident in the EIS measurements performed after 24 h of immersion time, as illustrated in Figure 1(b). Three capacitive loops were clearly observed: the first located between 100 kHz and 100 Hz, the second between 100 and 0.1 Hz and the third below 0.1 Hz. Therefore, one may conclude that, even at one-hour immersion, there may be three capacitive loops, but that these three loops are poorly separated.

The impedance diagrams can be modelled by three hierarchical capacitive loops (Figure 2(a)), and the parameter fitting was performed by a simplex method. The comparison between the model and experiment is presented in Bode format in Figure 2(b). The regression was applied only to the data obtained for the frequencies below 10 kHz because an inductive loop, unrelated to any actual electrode process, was observed in experimental data. The equivalent circuit used provided an adequate fit to the impedance data. The discrepancy between the experimental and the calculated data was within the estimated experimental error of ±1% of the

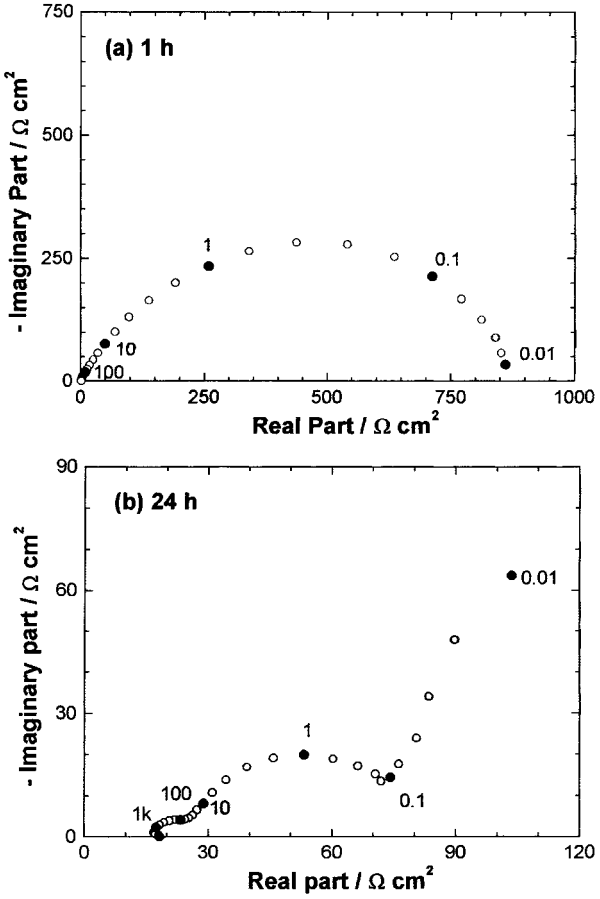

Fig. 1. Electrode impedance of Ni–P at open circuit: (a) after 1 h and (b) after 24 h immersion 1 M H_2SO_4.

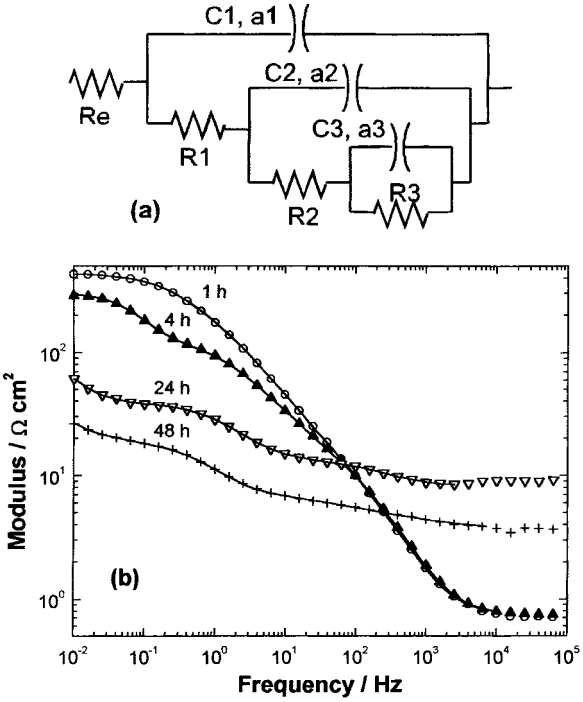

Fig. 2. Parameter fitting by a simplex method on data displayed in Figure 1. (a) Equivalent electrical circuit with three hierarchical *R–C* circuits. (b) Comparison of experimental and calculated data on the impedance modulus. (Experimental data: symbols; fitted data: curves).

modulus for both the real and the imaginary parts. As seen in Figure 2(b), the solution resistance (R_{sol}) obtained from the high-frequency limit of the impedance was small (0.75 Ω cm^2) for short immersion periods, $t \leqslant 4$ h. This value corresponds well to the solution resistance calculated from the resistivity of the test solution and the cell geometry. In contrast, at 24 h and 48 h of immersion, the high-frequency limit of the impedance was significantly higher. This phenomenon was attributed to deposition of corrosion products at the electrical contact between Ni–P alloy electrode and the alligator clip and thus has no relation with the electrode process.

The regressed parameter values for the three resistance–capacitance couples are presented in Figure 3 as a function of time. The parameters corresponding to the highest frequency loop (R_1–C_1) are presented in Figure 3(a). It can be seen that R_1 decreased while C_1 increased exponentially. The fitted equation obtained is shown together with calculated data from the electrode impedance. The initial value for C_1 is in agreement with that usually attributed to double layer capacitance. Its increase is attributed to the increase of the true surface area due partly to the roughening of electrode surface and also to the formation of the corrosion products (a grayish layer is visible to the naked eye). R_1, in parallel with the double layer capacitance, corresponds therefore to the charge transfer resistance (R_t). Because an oxidation–reduction process is considered to take place at the electrode interface, R_t is no longer related to the corrosion rate of Ni–P alloy, but to the exchange current density of oxidation–reduction reactions. The fitted results corresponding to the second capacitive loop are illustrated in Figure 3(b). In this figure, it can be seen that R_2 decreased while C_2 increased exponentially. The value of capacitance involved here is rather high, and it may be related to an oxidation–reduction process taking place at the electrode surface. This process is likely to take place in the corrosion products because the charge related to this redox process increased with time, in agreement with the change in R_1 and C_1. It is very likely that Ni^{2+}, formed by corrosion and remaining inside the corrosion products, leads to a redox process $Ni \rightleftharpoons Ni^{2+} + 2e^-$ ($E^\circ = -0.25$ V vs NHE) [13]. The evolution of the components of the R_3–C_3 couple are presented in Figure 3(c). Both R_3 and C_3 increase exponentially. The capacitance C_3 equal to 2 mF cm^{-2} at one-hour increased to 2 F cm^{-2} at 48 h immersion. R_3 is here closely related to the slope of the steady state current–potential curve, because the sum of the four resistances, $R_1 + R_2 + R_3$ is equal to the polarization resistance R_p. The increase in R_3 indicates that, after a long immersion period, the electrode becomes blocking in a manner corresponding to that encountered with a battery system. The origin of this time constant is still not understood, and will be discussed in our next work.

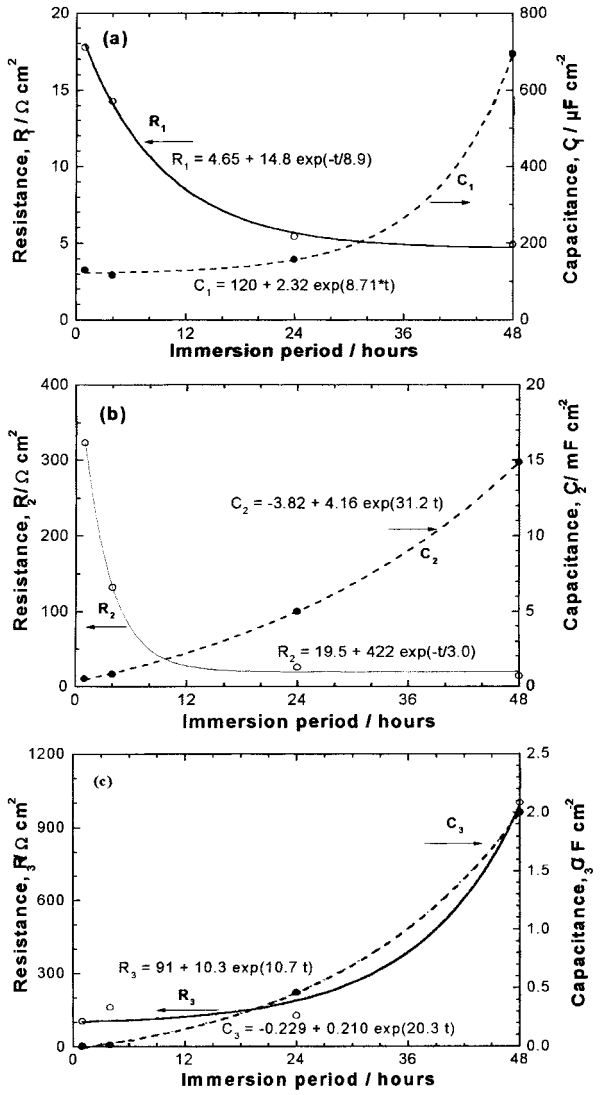

Fig. 3. Evolution of circuit elements at (a) $f > 10$ H_3 (highest range), (b) 10 Hz $< f <$ 1 Hz (medium range), and (c) $f <$ 1 Hz (lowest range), determined by fitting (Figure 2).

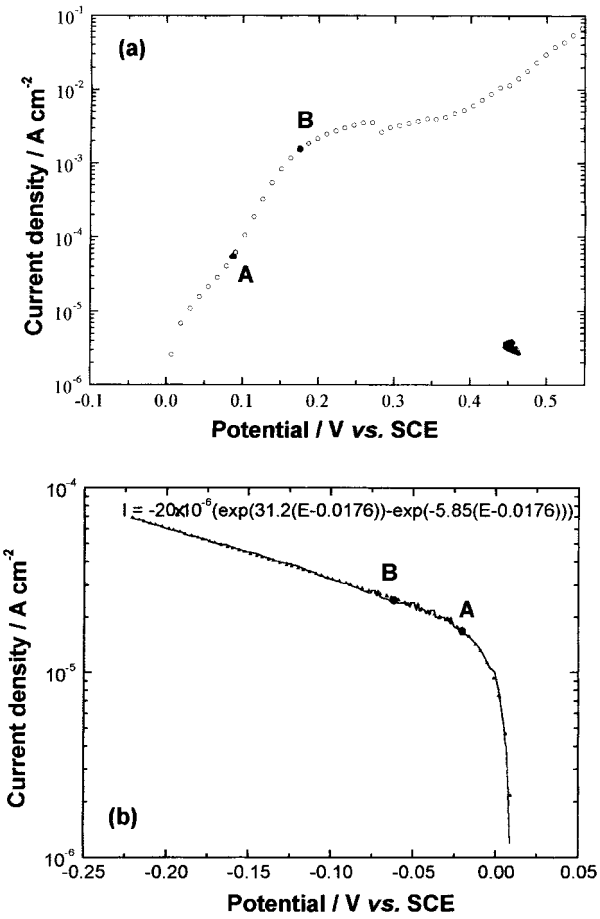

Fig. 4. Polarization curve of Ni–P alloy in 1 M H_2SO_4. Electrode priority maintained at the o.c.p. for 1 h before potential sweep at 0.5 mV s^{-1} (a) Anodic sweep and (b) cathodic sweep. Fitted data: curves.

3.1.2. *Polarization in the anodic domain.*
Electrode kinetics after one hour of immersion were examined by polarization curves and by impedance spectroscopy.

(a) *Polarization curves.* The anodic polarization curve obtained by the potential sweep method is presented in Figure 4(a). The anodic polarization characteristics are similar to those found by Carbajal and White [14] and Diegle et al. [15] for electrodeposited alloys in NaCl, HCl and H_2SO_4 environments. For potentials lower than 0.15 V vs SCE, two slopes were found, one up to 75 mV vs SCE where the Tafel slope β is 87 mV dec^{-1}, (or the Tafel coefficient $b = 27$ V^{-1}) and another one in the range 80–150 mV vs SCE giving $\beta = 50$ mV dec^{-1} (or $b = 47$ V^{-1}). The change in Tafel slope with applied potential can be explained by a reaction mechanism invoking two parallel reaction steps. When the electrode was left for a longer period at the open circuit, the first Tafel slope became difficult to observe. This may indicate that the second Tafel behaviour is more closely related to the oxidation of corrosion products. Beyond 150 mV vs SCE, the current exhibited a plateau ($I \approx 35$ mA cm^{-2}) which may be attributed to a diffusion-limited process. Three experiments with various electrode rotation speeds were performed (Figure 5). It was observed that the current value of the anodic plateau decreased slightly and the corrosion potential moved toward more positive values with an increase of rotation speed. This is in agreement with Zeller, but his results indicated an increase of the current density in agitated solution. He attributed that to a decrease of the film thickness with the agitation [6]. We assume that the slight decrease of the current plateau is due to a surface film becoming more homogenous, exposing less defected surface to the solution. The setting plateau is related to a film through which some ionic species can diffuse. Beyond this current plateau, a further current increase is observed.

(b) *Impedance diagram.* The impedance was measured at the foot (marked by point A) and at the top (marked B) of the second slope of the anodic polarization curve. The impedance diagram obtained at point A is presented in Figure 6(a), ($E = 87$ mV vs SCE) and $I = 53.2$ μA cm^{-2}). The diagram shows clearly two capacitive

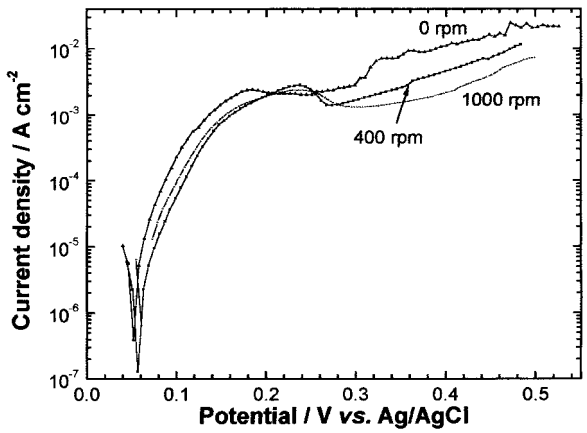

Fig. 5. Effect of rotation on current plateau. Electrode is first left in the test solution at o.c.p. for 1 h of immersion. $dE/dt = 0.5$ mV s^{-1}.

loops. The capacitance associated with the high frequency loop is equal to 55.6 μF cm^{-2}. This value is reasonably ascribed to the double layer capacitance. The parallel resistance, 214 Ω cm^2, is considered to be the charge transfer resistance R_t. Thus, the product of R_t by the current is equal to 11.4 mV, which is too small for a single irreversible reaction. For instance, the one encountered during the active dissolution of iron in this medium is 42 mV [16]. The small value of the product R_tI is consistent with the coexistence of two processes. Furthermore, the existence of a reversible electrode process is supported by the low-frequency capacitive loop, which had a capacitance equal to 11.0 mF cm^{-2}.

When the polarization potential approached the limiting current at the potential marked B in Figure 4(a) ($E = 176$ mV vs SCE, $I = 1.58$ mA cm^{-2}), the impedance diagram changed its shape drastically, as illustrated in Figure 6(b). The impedance diagrams reflect a capacitive loop ($f > 10$ Hz), an inductive loop though the imaginary part remains above the real axis ($10\ H_3 < f < 1$ Hz), and a second capacitive loop ($f < 1$ Hz). The capacitance at the high-frequency domain has a value of 33.2 μF cm^{-2} and is attributed to the double layer capacitance. The product of the charge transfer resistance by the d.c. current was 69 mV, therefore the influence of the backward reaction at this potential range is negligible.

The inductive loop was often encountered during active dissolution of metal, and was explained by a relaxation process of the reaction intermediate species. Since the electrode process is no longer reversible, the low-frequency capacitive loop is not related to the conservation of electrical charge as reaction product. This loop is related to the appearance of the current plateau. The reaction mechanisms in the anodic region and also the process leading to the current plateau are not yet clearly elucidated. Further investigation is needed, but we consider that this plateau is beyond the scope of the corrosion behaviour of Ni–P alloy. It may be probably be related to the alloy composition.

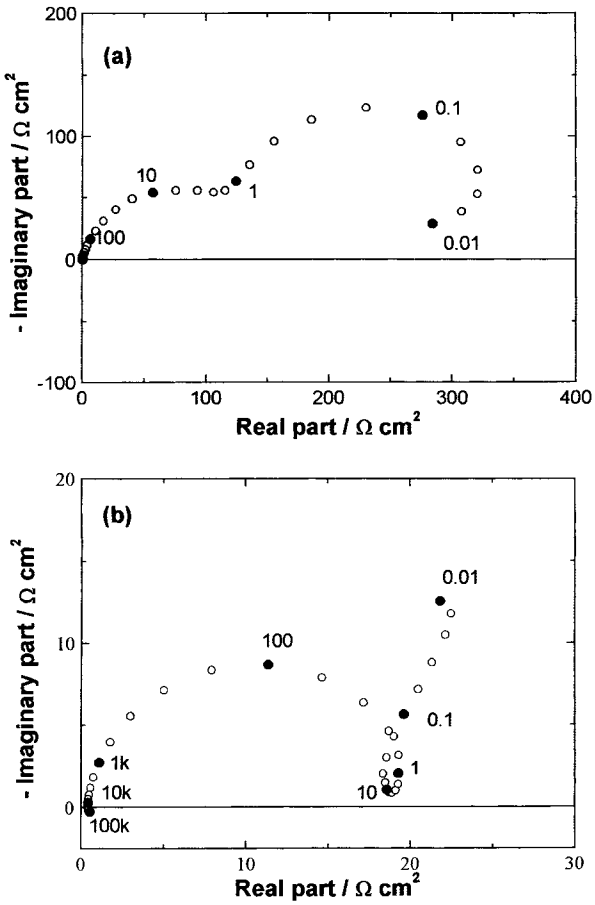

Fig. 6. Impedance diagrams obtained at (a) 0.087 V and (b) 0.176 V.

3.1.3. *Polarization in the cathodic domain*

(a) *Polarization curves.* The polarization curve in the cathodic domain is shown in Figure 4(b). The corrosion potential was slightly different from the one revealed in Figure 4(a), reflecting the lack of reproducibility of this corrosion system. This curve shows a wide potential range where the current follows the Tafel law. I_a, I_c and I_{corr} denote respectively the partial anodic, cathodic and the corrosion current. If both anodic and cathodic processes follow the Tafel law with coefficients b_a and b_c, then the overall current around the corrosion potential can be expressed by

$$I = I_a - I_c = I_{corr}[\exp(b_a\eta) - \exp(b_c\eta)] \quad (1)$$

where η is the overpotential:

$$\eta = E - E_{corr} \quad (2)$$

Nonlinear regression was performed to evaluate the parameters in Equation 1; the results are shown in Figure 4(b). The regressed value for E_{corr} was 0.0176 V vs SCE, I_{corr} was 20 μA cm^{-2}, b_c was –5.85 V^{-1}, and b_a was 31.2 V^{-1}.

(b) *Impedance diagram.* The EIS measurements illustrated in Figure 7 were obtained at the polarization

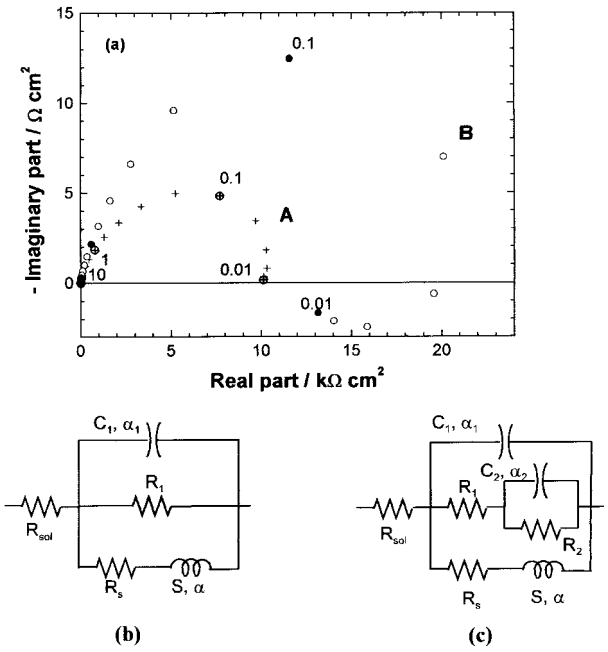

Fig. 7. (a) Impedance diagram obtained during cathodic polarization. (b) Inductive loop and (c) two capacitative and one inductive loop.

potentials A and B indicated in Figure 4(b). The impedance scans have one capacitive loop in the high-frequency range and one inductive loop in the low-frequency domain. The latter tended to appear when the potential became more cathodic. A parameter fitting involving an inductive loop, as depicted in Figure 7(b), was applied to these diagrams. The results of the fitting show a marked and systematic discrepancy in the transition range from capacitive to inductive loops. Since the impedance diagram at the corrosion potential was interpreted by three time-constants, an equivalent circuit involving two capacitive loops and an inductive one, depicted in Figure 7(c), was used for the regression analysis. In other words, when the electrode was polarized in the cathodic region, a capacitive loop located at the lowest frequencies range was transformed into an inductive one. The characteristic frequency corresponding to the apex of this loop was 30 mHz, close to that of the lowest frequency capacitive loop observed at the corrosion potential for one hour of immersion.

Some parameters calculated from the fitting procedures are summarized in Table 2. C_1 was on the order of 50 μF cm^{-2} at both potentials, therefore this capacitance was attributed to the double layer. R_1 was thus attributed to the charge transfer resistance. The product R_tI was equal to 74 and 5.3 mV, respectively, at potentials of −0.02 and −0.06 V vs SCE. At the higher potentials, it seems that an oxidation–reduction process involving H^+/H_2 or a phosphorus compound takes place. This oxidation–reduction process is indicated by a marked increase of C_2 with potential. The inductive loop observed may be associated with the lowest frequency capacitive loop observed at the corrosion potential. That is, when the overall current is positive, the process linked to this loop hinders the overall current; whereas, when the current is negative as a whole, the same process promotes it. A surface species will be reduced by active hydrogen and accelerate the cathodic process. Since this feature was observed on the Ni–P alloy, but not on the Ni electrode, the active surface species probably constituted of a phosphorus compound.

3.2. *Inhibiting effect of quaternary phosphine*

The inhibiting effect of triphenylalkyl-phosphine (P_3AP) on the corrosion of Ni–P alloy at different concentrations was examined in 1 M H_2SO_4 solution.

3.2.1. *At the open-circuit corrosion potential*

The impedance diagrams given in Figure 8 were obtained at the corrosion potential (E_{corr}) after one hour of immersion in the test solution. As was done for the solution without inhibitor, the electrical equivalent circuit depicted in Figure 2(a) was used to reproduce the impedance data shown in Figure 7. C_1 had a value of 307 and 25.1 μF cm^{-2} in presence of 5 and 20 mM of P_3AP, respectively. In the absence of the inhibitor and after one hour of immersion, C_1 was found equal to 130 μF cm^{-2}. The charge transfer resistance, parallel with C_1 was estimated to be 22 and 141 Ω cm^2 for 5 mM and 20 mM of P_3AP, respectively. Compared with the

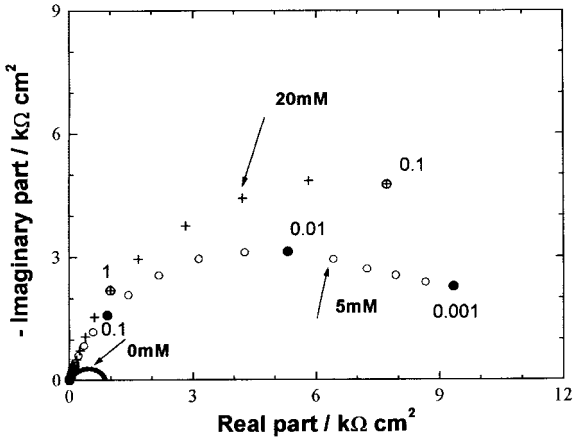

Fig. 8. Impedance diagrams at the corrosion potential for two different concentrations of P_3AP in 1 M H_2SO_4.

Table 2. Some parameters obtained by fitting calculation on the impedance data in the cathodic range

E/V vs SCE	C_1/μF cm^{-2}	R_1/Ω cm^2	C_2/μF cm^{-2}	R_2/kΩ cm^2	S/kH cm^{-2}	R_s/kΩ cm^2	χ^2
−0.02	59.4	4435	640	79.2	61.1	14.0	1.61
−0.06	44.9	220	1420	24.9	65.6	17.1	0.81

value of 17.8 Ω cm^2 found in the absence of P_3AP, it can be noticed that P_3AP decreases the reversibility of the oxidation–reduction process taking place at the electrode surface.

The capacitance C_2 was expected to be proportional to the amount of species involved in oxidation–reduction reactions. C_2 changes from 52.3 μF cm^{-2} in the absence of P_3AP to 20.2 and 27.3 μF cm^{-2} by addition of 5 mM and 20 mM of P_3AP, respectively, in 1 M H_2SO_4. The amount of corrosion products at the electrode surface decreases, but the effect of P_3AP seems to be rather to decrease the reactivity of these products.

3.2.2. *Polarization in the anodic domain*

Polarization measurements were used to examine how P_3AP modifies the electrode processes determining the corrosion of Ni–P alloy.

The polarization curves obtained by potential sweeping towards more positive potential after one hour of immersion are presented in Figure 9(a). The initial polarization potential was close to E_{corr}. The corrosion potential E_{corr} shifted towards more anodic potentials with increasing P_3AP concentration up to 10 mM, and then towards more negative values beyond this concentration. The current value at the current plateau decreased dramatically beyond this critical concentration. The current plateau became about 100 times lower than that observed in the absence of the inhibitor. This plateau is related to the formation of a surface layer due to the anodic dissolution of Ni–P alloy in the absence of inhibitor, but the formation of surface film is enhanced by the presence of P_3AP. Indeed, one observes by the naked eye that, in the presence of P_3AP, the electrode surface is covered by a white layer instead of the grayish layer found in its absence. This precipitation, therefore, hinders dramatically the dissolution of Ni–P alloy. In presence of the inhibitor, the current plateau appeared at a less anodic potential. At lower concentrations, a good efficiency was obtained close to E_{corr} while at higher levels, the phosphonium salt had a stimulating effect on the anodic process.

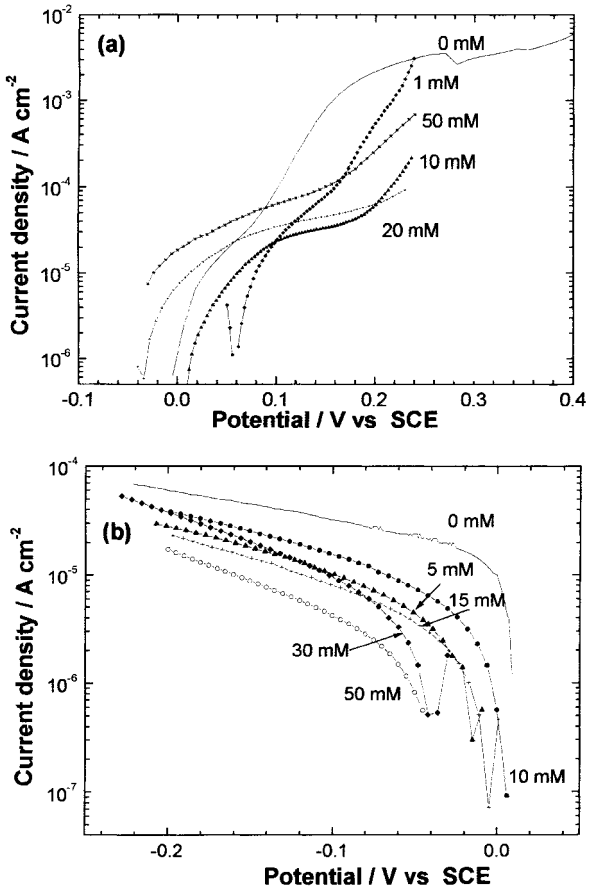

Fig. 9. Effect of various concentration of P_3AP in both (a) anodic and (b) cathodic region. Sweep rate 0.5 mV s^{-1}.

3.2.3. *Polarization in the cathodic domain*

The polarization curves obtained by the potential sweep toward more negative values after one hour of immersion at open circuit potential are presented in Figure 9(b). The initial potential was close to the corrosion potential observed during the anodic sweeps.

The shape of the curves was the same as that found in the absence of inhibitor, and the corrosion potential shifted to more negative values when concentration of P_3AP was increased.

A nonlinear regression was used to calculate the different parameters defined by Equation 1. The results of fitting procedure are displayed in Table 3. I_{corr} decreased markedly with the inhibitor concentration in agreement with the results shown in Figure 8. The b_a values decreased when the P_3AP concentration was increased, while the magnitude of b_c increased slightly. As the P_3AP concentration is increased, the inhibiting effectiveness of P_3AP as a corrosion inhibitor of Ni–P alloys was enhanced. An inhibitor efficiency of 90% was recorded at the inhibitor concentration of 50 mM.

4. Conclusions

The combined electrochemical methods used in the present work permitted the characterization of the corrosion behaviour of Ni–P alloy obtained by electroless plating in 1 M H_2SO_4 solution.

The polarization curves revealed in the cathodic region a Tafel behaviour. In contrast, in the anodic domain, two different slopes were observed near E_{corr}, followed by an establishment of a current plateau. The

Table 3. Some parameters obtained by fitting calculation on polarization curves in presence of P_3AP in cathodic range

Concentrations/mM	I_{corr}/A cm^{-2}	b_a/V^{-1}	b_c/V^{-1}	E/%
0	20	31.2	−5.85	–
5	7.8	6.6	−7	61
10	3.6	28.71	−8.34	82
15	4	9.6	−9.6	80
30	5.5	17	−12	72
50	2	24	−13	90

two anodic Tafel slopes can be attributed to two reaction steps taking place in parallel; whereas, the current plateau is associated with a film formation rather than a diffusion limiting process.

The impedance spectra suggested that dissolution of this specimen was characterized by three time constants, which were initially difficult to distinguish but were clearly observable after a long immersion period.

An oxidation–reduction process involved by the corrosion products takes place at the electrode interface. The Ni^{2+} formed by corrosion process remains within the corrosion product layer and give rise to a redox process Ni/Ni^{2+}.

P_3AP is an effective corrosion inhibitor of Ni–P alloy in 1 M H_2SO_4. Tafel extrapolation of cathodic polarization curves showed that inhibiting efficiency reached 90% at the concentration of 50 mM. In anodic polarization curves, the current plateau value was reduced by a factor of 100 when the inhibitor was added at the concentration of 10 mM. Even though the behaviour of the inhibitor could not be neglected in the anodic domain, a greater effect of the phosphonium species was observed in the cathodic region.

Acknowledgements

S. O. N. thanks ISESCO for his fellowship. The authors wish to express their gratitude to Professor Orazem for his help in the realization of this manuscript.

References

1. J. Chitty, A. Pertuz and H. Hintermann, *Thin solid films* **308–309** (1997) 430.
2. A.G. Revesz and J. Kruger, *in* R.P. Frankenthal (Ed), 'Passivity of Metals' (Electrochemical Society, NJ, 1978), p. 137.
3. P. Marcus and O. Oda, *Mem. Sci. Rev. Metall.* Nov. (1979) 715.
4. R.H. Jones, M.J. Danielson and S.M. Bruemmer, *in* R.P. Gangloff (Ed), 'Embrittlement by the Localized Crack Environment' (TMS-AIME, Warrendale, PA, (1994), p. 419.
5. R.B. Diegle, N.R. Sorensen and G.C. Clayton, *J. Electrochem Soc.* **133** (1986) 1769.
6. R.L. Zeller, *Corros. Sci.* **47** (1991) 692.
7. P. Cadet, M. Keddam and H. Takenouti, *in* M. Froment (Ed), 'Passivity of Metals and Semiconductors' (Elsevier, Amsterdam, 1983), p. 311.
8. M. Cherkaoui, A. Srhiri and E. Chassing, *Plat. Surf. Finish.* **79** (1992) 68.
9. M. Cherkaoui, A. Srhiri and E. Chassing, *J. Appl. Electrochem.* **23** (1993) 1169.
10. M.E. Touhami, E. Chassing, M. Cherkaoui, A. Srhiri and A. Ben Bechir, *J. Appl. Electrochem.* **26** (1996) 487.
11. M.E. Touhami, E. Chassing, and M. Cherkaoui, *Electrochim. Acta* **43** (1998) 1721.
12. M. Makoza, 'Modern Synthetic Methods Waked Anions, phase transfer', IUPAC, **7** (1976).
13. W.M. Latimer, 'Oxidation Potential', 2nd edn (Prentice-Hall, Englewood Cliffs, 1952).
14. J.L. Carbajal and R.E. White, *J. Electrochem. Soc.* **135** (1988) 2952.
15. R.B. Diegle, N.R. Sorensen, G.C. Clayton and M.A. Helfand, R.B. Diegle and K. Hasimoto (Eds), 'Corrosion electrochemistry and catalysis of metallic glasses', The Electrochemical Society, **88-1** (1988).
16. I. Epelboin and M. Keddam, *J. Electrochem. Soc.* **17** (1970) 1052.